# Fluorescence Imaging of Local Membrane Electric Fields during the Excitation of Single Neurons in Culture

Paul Gogan, Ingrid Schmiedel-Jakob, Yasmina Chitti, and Suzanne Tyč-Dumont
Unité de Neurocybernétique Cellulaire, CNRS UPR 418, 13009 Marseille, France

ABSTRACT The spatial distribution of depolarized patches of membrane during the excitation of single neurons in culture has been recorded with a high spatial resolution (1 $\mu m^2$/pixel) imaging system based on a liquid-nitrogen-cooled astronomical camera mounted on an inverted microscope. Images were captured from rat nodose neurons stained with the voltage-sensitive dye RH237. Conventional intracellular microelectrode recordings were made in synchrony with the images. During an action potential the fluorescence changes occurred in localized, unevenly distributed membrane areas, which formed clusters of depolarized sites of different sizes and intensities. When fast conductances were blocked by the addition of tetrodotoxin, a reduction in the number and the intensities of the depolarized sites was observed. The blockade by tetrodotoxin of voltage-clamped neurons also reduced the number of depolarized sites, although the same depolarizing voltage step was applied. Similarly, when a voltage-clamped neuron was depolarized by a constant-amplitude voltage step, the number of depolarized sites varied according to the degree of activation of the voltage-sensitive channels, which was modified by changing the holding potential. These results suggest that the spatial patterns of depolarization observed during excitation are related to the operations of ionic channels in the membrane.

## INTRODUCTION

The excitability of neurons is associated with a variety of channels governing the flow of ionic current across the plasma membrane (Llinás, 1988). Channels are becoming well understood as a result of powerful tools such as patch clamping, molecular cloning, and site directed mutagenesis, which allow single-channel behavior to be analyzed (Catterall, 1988; Unwin, 1989; Miller, 1991; Stühmer, 1991; Hille, 1992). It is well established that action potentials are generated by voltage-sensitive $Na^+$ channels; $K^+$ conductances as well as $Na^+$ inactivation contribute to repolarizing the membrane after the action potential. In addition, a large body of data has demonstrated the multiple roles of calcium in the control of fundamental functions in neurons. In particular, calcium imaging has stressed the importance of the nonuniform spatial distribution of calcium concentration in a variety of neuronal activities (Connor, 1986; Regehr et al., 1989; Ross et al., 1990; Sugimori and Llinás, 1990; Schilling et al., 1991; Llinás et al., 1992; Miyakawa et al., 1992; Tauc, 1992; Wadman and Connor, 1992; Bacskai et al., 1993; Midtgaard et al., 1993; Verderio et al., 1994; Zheng et al., 1994). However, the spatial pattern of electrical activity in neurons remains unknown because of the restriction imposed by conventional single site microelectrode recording. Clearly, it would be of great interest to refine measurement techniques to resolve discrete changes in local field potential that might be expected to occur when channels open or close in the plasma membrane of single neurons.

Over the past 20 years it has become possible to detect and to measure rapid transient changes in membrane potential by using voltage-sensitive dyes as optical probes (for references see Grinvald et al., 1988; Cohen et al., 1989). Fluorescent styril dyes were originally introduced by Loew and co-workers (1979) and by Grinvald and co-workers (1982, 1983) as electrochromic dyes for the optical recording of membrane potentials at high temporal resolution (Ross et al., 1977; Grinvald et al., 1982; Gross et al., 1986). Bath-applied dye binds to the external membrane and acts as a molecular transducer, transforming changes in membrane potential into optical signals. Furthermore, it has been shown that the fluorescence of the stained neuron correlates linearly with its electrical activity recorded with a microelectrode (Chien and Pine, 1991; Fromherz et al., 1991). Recently, fluorescence signals from the RH series of styril dyes were shown to become incorporated into membranes containing Na, K-ATPase and have been used to monitor transitions between different states of the pumping cycles (Klodos and Forbush, 1988). More recently, Bühler et al. (1991) reported that some styril dyes respond mainly to local changes of field strength in the membrane and suggested that the most probable explanation of their findings is that the dye acts as an electric field sensor.

In this report we describe a system for detecting small changes in the fluorescence of voltage-sensitive dyes, using a liquid-nitrogen-cooled astronomical CCD camera mounted on an inverted microscope. The large dynamic range, ultrahigh sensitivity, and low noise associated with such a system allow the detection of very small fluorescence changes. We present here the first topographical images of the spatial domain of the excitation of single neurons in culture with the styril dye RH237 as a molecular sensor of local electric fields. The patchiness of the distribution of the depolarized sites confirms the importance of exploring this

*Received for publication 18 January 1995 and in final form 19 May 1995.*
Address reprint requests to Dr. Suzanne Tyč-Dumont, Unité de Neurocybernétique Cellulaire, CNRS UPR 418, 28 boulevard Sainte-Marguerite, 13009 Marseille, France. Tel.: 33–91-75–02-00, Fax: 33–91-26–20-38.
© 1995 by the Biophysical Society
0006-3495/95/08/299/12 $2.00

space dimension on the microscopic scale and opens the way to the study of assemblies of functionally discrete domains of neuronal excitation at the level of single neurons. Preliminary accounts of these results were reported previously (Gogan et al., 1991; Rioult et al., 1991; Gogan and Tyč-Dumont, 1994; Chitti et al., 1995).

## MATERIALS AND METHODS

Experiments were performed on dissociated neurons from the rat nodose ganglion, which were prepared by the procedure described by Ikeda et al. (1986) with slight modifications. Wistar rats 4 to 10 days old were killed (after ether anesthesia) by cervical dislocation, and the nodose ganglia were removed and placed in a Hanks balanced salt solution supplemented with 5-mM *N*-2-hydroxyethylpiperazine-*N'*-2-ethanesulfonic acid and penicillin/streptomycin (100 μg/ml). For dissociation, the ganglia were transferred to a Hanks balanced salt solution containing trypsin (8–12 U/ml), collagenase A (0.5 U/ml), and DNase I, grade II (200 U/ml) and gently triturated over a period of 10–30 min to release neuronal somata from the ganglia. The cell suspension was spun down and resuspended in a modified Hanks balanced salt solution containing bovine serum albumin (0.7 mg/ml), 10% fetal calf serum, and 2.5-mM $CaCl_2$. After centrifugation, the cells were resuspended in a culture medium (Dubelcco's minimum essential medium/nutrient mix F12, 1:1, supplemented with a cocktail containing $NaCO_3$ (14 mM), transferrin (100 μg/ml), insulin (5 μg/ml), putrescin (100 nM), progesterone (20 nM), oestradiol (1 pM), sodium selenite (30 nM), glucose (33 mM), glutamine (2 mM), penicillin/streptomycin (100 μg/ml), and heat-inactivated fetal calf serum (3%) and plated at low density (200–300 cells) on glass cover slips coated with poly-L-Lysine. The cultures were incubated at 37°C in a 95% air, 5% $CO_2$ atmosphere and maintained for 6 to 24 days.

For experimentation, the cover slip carrying the culture was sealed with a rubber gasket to the Perspex recording chamber (total volume 2 ml), creating a transparent bottom. The culture was continuously superfused with a normal bath solution containing (in mM) 140 NaCl, 4 KCl, 2 $MgCl_2$, 2 $CaCl_2$, 10 *N*-2-hydroxyethylpiperazine-*N'*-2-ethanesulfonic acid. Osmolarity was adjusted to 310–320 mosm/kg with glucose, and pH was adjusted to 7.3–7.4 with NaOH. Superfusion was done between two pipettes positioned opposite each other. When used, tetrodotoxin (Sigma, Quentin Fallavier, France) was added directly to the chamber.

The voltage-sensitive styril dye RH237 (Molecular Probes, Eugene, OR), dissolved in DMSO to make 1-mM stock solutions and kept refrigerated in tightly capped tubes, was diluted just before use in recording bath solution to 0.5–2 μM. Cultures were stained by replacement of the bath solution by the desired dye concentration for 10 min followed by washing for 20 min with the standard medium to remove unbound dye. Staining was considered adequate when the cells showed a bright fluorescent ring on focusing on their equators. This bright outline of the cell indicated that dye-binding was restricted to the plasma membrane. Experiments started 15–30 min after washing. All experiments were performed at room temperature (23–25°C) measured in the bath.

### Electrophysiological recording

Conventional intracellular microelectrodes were filled with 1-M K-acetate and had resistances of 60–100 MΩ. Single electrode voltage and current-clamp was accomplished with a bridge amplifier (Axoclamp 2A, Axon Instruments, Foster City, CA). Data were stored in a computer using a CED1401-plus interface (Cambridge Electronic Design, Cambridge, UK). The intracellular recordings were synchronized with CCD image acquisition (Fig. 1). During recording sessions the neurons were usually held hyperpolarized at approximately −100 mV to maintain the membrane potential stable. The electrophysiological properties of some nodose neurons were evaluated by whole-cell patch clamp techniques during in vitro development for up to 7 weeks in culture. The average resting membrane

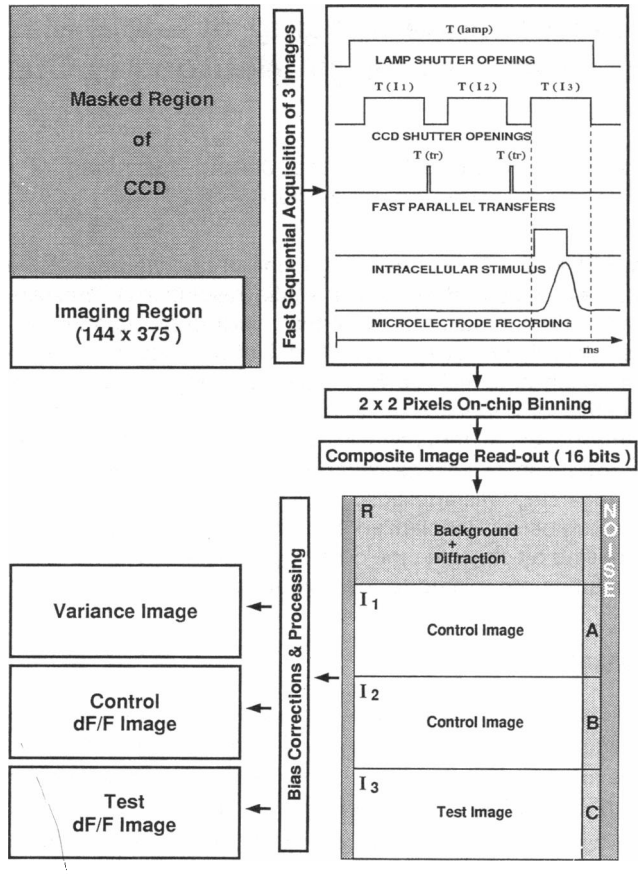


FIGURE 1 Diagram illustrating the image acquisition system. (*Upper left*) A mask placed in the conjugate image plane covers the CCD (578 × 385) except for a rectangular slit of 144 × 375 pixels (imaging region). The masked region of the CCD is used as a storage area. (*Upper right*) Timing diagram for fast sequential acquisition. The preparation is illuminated over a period $T$ (lamp). Three images are taken in sequence with exposure times $T(I_1) = T(I_2) = T(I_3)$ adjusted to include the action potential recorded by the intracellular microelectrode. After each exposure the image is shifted into the masked region of the CCD by fast parallel charge transfer ($T$(tr) = 1 ms). At the beginning of $T(I_3)$ an intracellular stimulus is triggered and the time course of the excitation of the neuron is recorded in synchrony with conventional electrophysiological technique. The charges on 2 × 2 pixels were added before readout (on-chip binning) 16 bits digitized and stored in the computer memory. (*Lower right*) The resulting composite image contains a reference area, R, with background noise and diffraction artifacts that are due to the slit, two control images, $I_1$ and $I_2$, and the test image, $I_3$. The three areas A–C contain measurements of fluorescence intensity used to correct shutter open time instability and dye bleaching. The two additional areas (dark shading: *left*, 10 pixels; *right*, 20 pixels) contain a measure of the system noise for each row of the composite image (*NOISE*). (*Lower left*) The variance of every pixel in the test d$F/F$ image is computed by inclusions of all sources of noise (variance image). The control of d$F/F$ image is obtained by computing $(I_1 - I_2)/I_1$. An image of the neuronal response is displayed (test d$F/F$ image) by computing $(I_2 - I_3)/I_2$.

potential was −58.2 ± 2 mV ($n$ = 38). On brief depolarization all neurons responded with at least one overshooting action potential that had a mean threshold of −32 mV (Schmiedel-Jakob et al., 1992). In the present experiments our intracellular recordings, before staining, were similar and revealed the two distinct populations of nodose neurons described in vivo by Gallego and Eyzaguirre (1978) and in vitro by Ikeda et al. (1986) and Schild et al. (1994). One neuron type displayed a short duration action potential (3–5 ms) and was less frequently observed than the other type,

which exhibited longer action potentials (6–12 ms). Our observations (see Fig. 3 below) agree quite well with earlier reports (Baccaglini and Cooper, 1982; Higashi et al., 1984; Schild et al., 1994).

## Optical assembly

The optical system was built around a Zeiss Axiovert 35 M inverted microscope mounted on a large *X/Y* table to allow the imaging axis to move independently of the preparation. The cover slips carrying the cultures had a thickness of 0.17 (+0.01 or −0.03) mm and a refractive index of 1.542 ± 0.003 at 546 nm. The chamber was mounted on a heavy stage and attached, together with the micromanipulators, to a rigid frame. The entire assembly was placed on an air table (Newport Corp., Irvine, CA) to isolate it from vibrations.

The light source was a 100-W mercury lamp highly stabilized by photofeedback (Oriel, Stratford, CT), providing illumination via a 1-mm-diameter quartz fiber. An electronic shutter (Uniblitz, Rochester, NY; VS25 shutter and D122 driver) controlled the illumination times. The intensity of the light was adjusted by appropriate neutral-density filters placed in in the light path. The light was band-passed by an interference filter (546 ± 6 nm), reflected by a dichroic mirror (570 nm), and focused on the preparation with a 40×, N.A. 1.3, oil immersion objective lens (Zeiss Plan Neofluar). The immersion oil (Zeiss 518C) matched the optical characteristics of the objective lens and the coverslips at 23°C. The fluorescent light was collected by the same objective lens, passed through the dichroic mirror, band-limited by a long-pass filter (≥610 nm), then projected onto a CCD photodetector array through the upper optical port of the microscope. The final image resolution was 0.5 × 0.5 μm per pixel. An auxiliary conventional video CCD camera was attached to the side optical port for precise focusing.

## Imaging system

The imaging system consisted of a modified astronomical camera (Astromed, Cambridge, UK). The detector array, a 578 × 385 pixels P8600 CCD chip (EEV Ltd., Chelmsford, UK) was placed inside a Dewar (MN 1815 INV, Oxford Instruments, Oxford, UK), filled with liquid nitrogen and thermally isolated by high vacuum ($<10^{-6}$ hPa). The exposure time was controlled by an electronic shutter identical to that for the light source, placed in front of the chip. The chip control electronics (Astromed 2200) were linked to a RISC computer (Fast Firmware Techniques, Southampton, UK) with a cycle time of 176 ns, allowing fast interaction with the CCD and external apparatus and flexible control of the charges accumulated by the chip. Selection of readout area, on-chip binning before readout, and on-chip storage of image sequences were available. The low-noise image readout was obtained by a dual slope integration procedure and analog to digital conversion with 16-bit resolution. The entire imaging system was controlled by a 486/33 computer with UNIX, with image storage on a 600-Mbyte magneto-optical disk.

The system had a noise level of fewer than 10 electrons root mean square and a linear flux detection range from 1 (photon/pixel)/min to $10^9$ (photons/pixel)/s. The programmable gain gave a dynamic range of $10^5$:1. The exceptional light sensitivity ($10^{-11}$, lux) and low noise of the system allowed the use of reduced intensity of the incident light and dye concentration, thus reducing photobleaching and phototoxicity.

## Mechanical stability and cell movements

The high spatial resolution of the system necessitated a high degree of mechanical stability to avoid movement artifacts. The vibrations provoked by the opening of the illumination shutter were suppressed by placement of the lamp and illumination shutter in a remote position from the microscope, and optical coupling was obtained by an optic fiber. The CCD shutter was fixed in a high-inertia plate and suspended inside the shutter enclosure by three fine nylon threads.

To retain the high sensitivity and low noise detection capabilities of our CCD system, the chip had to be read out at slow speed (4 to 8 s, depending on the pixels' binning strategy). This was not consistent with comparing successive images of the stimulated and unstimulated neuron. Such comparison was necessary to detect fractional changes in fluorescence ($dF/F$ in percent) linked to localized electrical events in the plasma membrane. With long intervals, the computed image could be composed mainly of patterns produced by cell movements between the two images (Pratt, 1991). To avoid this problem we implemented a procedure that permitted recording a fast sequence of images while maintaining low noise, high accuracy, and slow scan read out.

## Fast sequential imaging

The region of interest in the preparation was imaged on part of the CCD (144 × 375 pixels) through an adjustable rectangular slit in a mask placed in the conjugate image plane. The masked area on the CCD (Fig. 1, upper left) was used to store successive images, which were fast shifted into the storage area by parallel charge transfer between exposures. The band (10 pixels wide) to the right of the imaging area was used to store information on the illumination level of each image, giving after readout bands A–C (Fig. 1, lower right). We exposed each image by opening the CCD electronic shutter for a duration adjusted to include the action potential (Fig. 1, upper right). When the first image was taken the diffraction that was due to the slit affected some pixels in the masked area, which were kept for further correction of the images. When the second and third images were taken the diffraction affected pixels in the first and second images, respectively. At the end of a sequence the CCD contained four areas: one with the background noise (dark noise) and the diffraction pattern and three with successive images of the neuron. The total duration of the recording sequence was less than 100 ms (Fig. 1, upper right). Then the CCD was read out at slow speed (~4 s) after 2 × 2 pixel on-chip binning was performed. The advantage of the 2 × 2 binning was that the signal readout was larger by a factor of 2 × 2 = 4 but had only one unit of readout noise added by the output amplifier, resulting in a final image resolution of 1 $\mu m^2$/pixel with an increased signal-to-noise ratio. At the end a composite image was obtained that contained one area (R) with background noise and diffraction pattern, two control images ($I_1$, $I_2$; neuron at rest), a test image ($I_3$; excited neuron) and three areas A–C, containing supplementary information for computing corrections for the shutter open time instability and bleaching (Fig. 1, lower right). The serial output register of the CCD contained more pixels than one row in the imaging area. Because these additional dark pixels provided an excellent dark reference signal, 30 of these pixels were added to each row during readout, generating two supplementary lateral bands (Fig. 1, lower right, NOISE), giving the measure of the apparatus's dark noise and readout noise.

## Image processing

Image analysis was performed on a UNIX workstation with a suite of custom imaging software developed by Astromed (IMAGER) and on a SUN IPX graphic workstation with ESO-MIDAS, a software developed by the European Southern Observatory (Garching, Germany) for processing astronomical images and data. The dark noise, the readout noise, and the diffraction artifacts (derived from area R, Fig. 1) were subtracted from images $I_1$, $I_2$, and $I_3$, which we corrected for illumination shutter open time variation and dye bleaching by using scaling coefficients evaluated from measurements stored in the A, B, and C areas, respectively, in the image (Fig. 1).

The fractional changes in fluorescence $dF/F$ were computed pixel by pixel for the control and test conditions: control $dF/F = (I_1 - I_2)/I_1$ and test $dF/F = (I_2 - I_3)/I_2$. Because of the extremely low instrumental noise generated by the recording system, the noise in the images was entirely dominated by the shot noise that resulted from random fluctuations in the rate of arrival of photons at the CCD surface. Thus the noise in the computed $dF/F$ images was inversely proportional to the square root of the pixel intensities in the original images. As the fluorescence intensity of the stained neuronal membrane was 10 to 30 times higher than the background fluorescence, the noise in the $dF/F$ images was 3 to 5 times larger for the

background than for the neuron. This relative enhancement of the background noise impaired the visualization of the changes in fluorescence that were due to neuronal excitation (Fig. 2 *B*). Two treatments were used to help visualization. In the first treatment, background noise was reduced by an adaptative filter based on the "outlier" local gradient method described by Pratt (1991). Each pixel was compared with the average of its eight neighbors. If the magnitude of the difference was greater than some threshold level, the pixel was judged to be noisy and replaced by its neighbors average or set to zero (Fig. 2 *D*). The threshold was easily chosen in our conditions because of clear-cut differences in the statistical properties (different variances) of background and stained membrane areas in the image (Fig. 2 *C*). A second treatment consisted of spatial smoothing with a square (3 × 3) median filter (Tukey, 1971; Pratt, 1991), which displayed pixel clusters with significantly similar intensities (Fig. 2 *E*).

To verify the reliability of the clusters revealed by our treatments, we computed the variance ($V(x, y)$) of each pixel in the processed d$F/F$ image, taking into account all sources of variance introduced by shot noise, instrumentation, and image processing (Fig. 2 *C*). The intensity $I$ of each pixel in the original fluorescence image is a Poisson variable with a variance $\sigma^2 = I + N$, where $I$ is the shot noise and $N$ takes into account the dark and the readout noise. In the final d$F/F$ images the variance of each pixel is expressed by

$$V(x, y) = V\left(\frac{i_2 - i_3}{i_2}\right)$$

$$= \frac{i_3^2}{i_2^4}\left[C_1^2 I_2 + C_1^2 C_2^2 I_R + C_1^2(1 + C_2^2)N\right] + \frac{1}{i_2^2}(I_3 + N),$$

where $I_2$ and $I_3$ are the intensities of each pixel in the raw control and test images, respectively, $i_2$ and $i_3$ are the intensities of each pixel in the control and test images, respectively, after correction for instrumental errors, $I_R$ is the intensity of each pixel in the reference image (background noise and diffraction artifact), $C_1$ and $C_2$ are correction factors for bleaching and shutter open time instability obtained from lateral bands A–C in the image (see Fig. 1), and $N$ is the variance of the dark and readout noise of the system obtained from the supplementary noise bands. The d$F/F$ values of the pixels in the images were grouped into classes in steps of 0.3%. The spatial coordinates of the pixels belonging to each class were identified in the filtered image. Then, using the pixel values of the unfiltered d$F/F$ image, we computed the mean value and the total variance of each class, taking into account the computed $V(x, y)$. The means were compared by use of the robust Bienaimé–Chebyshev theorem (Parzen, 1960). The results showed that differences between cluster means were significant in a 80–99.9% confidence limit. We also used an analysis of hierarchized structures based on the wavelet transform (Grossmann and Morlet, 1985; Holdschneider et al., 1989; Bijaoui, 1992), which was developed to detect objects and clusters of structures in astronomical images of galaxies. Recent algorithms implementing the wavelet transform (Holdschneider et al., 1989; Worrall et al., 1992; Slezak et al., 1993; Starck and Bijaoui, 1994a,b), available in ESO-MIDAS software, allow for linear image decomposition, elimination of noise, and detection of statistically significant structures (see Fig. 4 below).

## RESULTS

### Intracellular recordings

Some neurons were impaled before staining with RH237 to test the stability of intracellular recordings in the culture (Fig. 3). Some neurons were recorded before, during, and after staining to evaluate the possible damage produced by the dye (Fig. 3 *A* and *B*). After staining, the mean membrane resting potential was −58.7 ± 2.5 mV ($n$ = 45). In most cells action potentials were evoked by depolarizing current pulses (0.1–1.5 nA), as shown in Fig. 3. On occasion, after illumination of the stained culture, we observed a depolarization of variable degree depending on the cell despite the low illumination level used in our experiments. This apparently photodynamic effect was not systematically studied. Typically, this effect was manifested as an increase in the duration of the action potential to as long as 65 ms. The fast $Na^+$ component remained unaffected (Fig. 3 *C* and *D*). Because the aim of these experiments was to reveal changes in patterning of the fluorescence with excitation of the neuron, we also tested neurons that had the low resting potential of −30 mV. Such cells, hyperpolarized with injected current, showed normal action potentials when stimulated. They also showed shifts in fluorescence patterning in the same way as neurons having more negative initial resting potential. These observations indicate that the behavior of the patterning was independent of possible impalement damage.

### Simultaneous intracellular and optical recordings

The standard protocol consisted of comparing processed d$F/F$ images of a single neuron under different experimental conditions. When a nodose neuron stained with RH237 was stimulated intracellularly with a depolarizing current pulse it typically responded with an action potential, and simultaneous changes in RH237 fluorescence were detected in all recorded neurons ($n$ = 106). The sign of the fluorescence variation was in agreement with electrophysiological studies on cells stained with RH237 or RH421: the styril dye responded to a membrane depolarization with a recorded fluorescence decrease (Grinvald et al., 1982, 1983; Müller et al., 1986). Examples of two impaled neurons imaged during their excitation and at rest are illustrated Fig. 4, in which *A* and *G* show the fluorescence CCD images of two different cultures. Both fields contained numerous stained processes surrounding the impaled neurons. In Fig. 4 *G* a heavily stained neuron can be seen close to the impaled neuron. The color images represent the high spatial resolution imaging of the relative fluorescence changes (d$F/F$%) in the same fields as in Fig. 4 *A* and *G* during the time course of the action potential. These images processed with the local gradient plus median filtering method reveal that the changes in fluorescence are restricted to the excited neuron, whereas all the surrounding processes and cell bodies are devoid of significant signal (Fig. 4 *B*, *C* and *H*, *J*). In particular, there is no change in fluorescence in the unstimulated heavily stained neuron located at the left of the impaled neuron in *G*. The distribution of depolarized membrane sites displays fluorescence clusters of different sizes and intensities, creating a patchy appearance on the neuronal membrane. Computations with the Bienaime–Chebyshev theorem show that the clusters are statistically significant, with 99.9% confidence limits. Surprisingly, the spatial distribution varied between images, as seen, for example, in Fig. 4 *C* taken 23 s after *B* and despite the production of superposable action potentials (Fig. 4 *F*). Clusters of depolarized sites were also observed on the neurites with heterogeneous and variable spatial distribu-

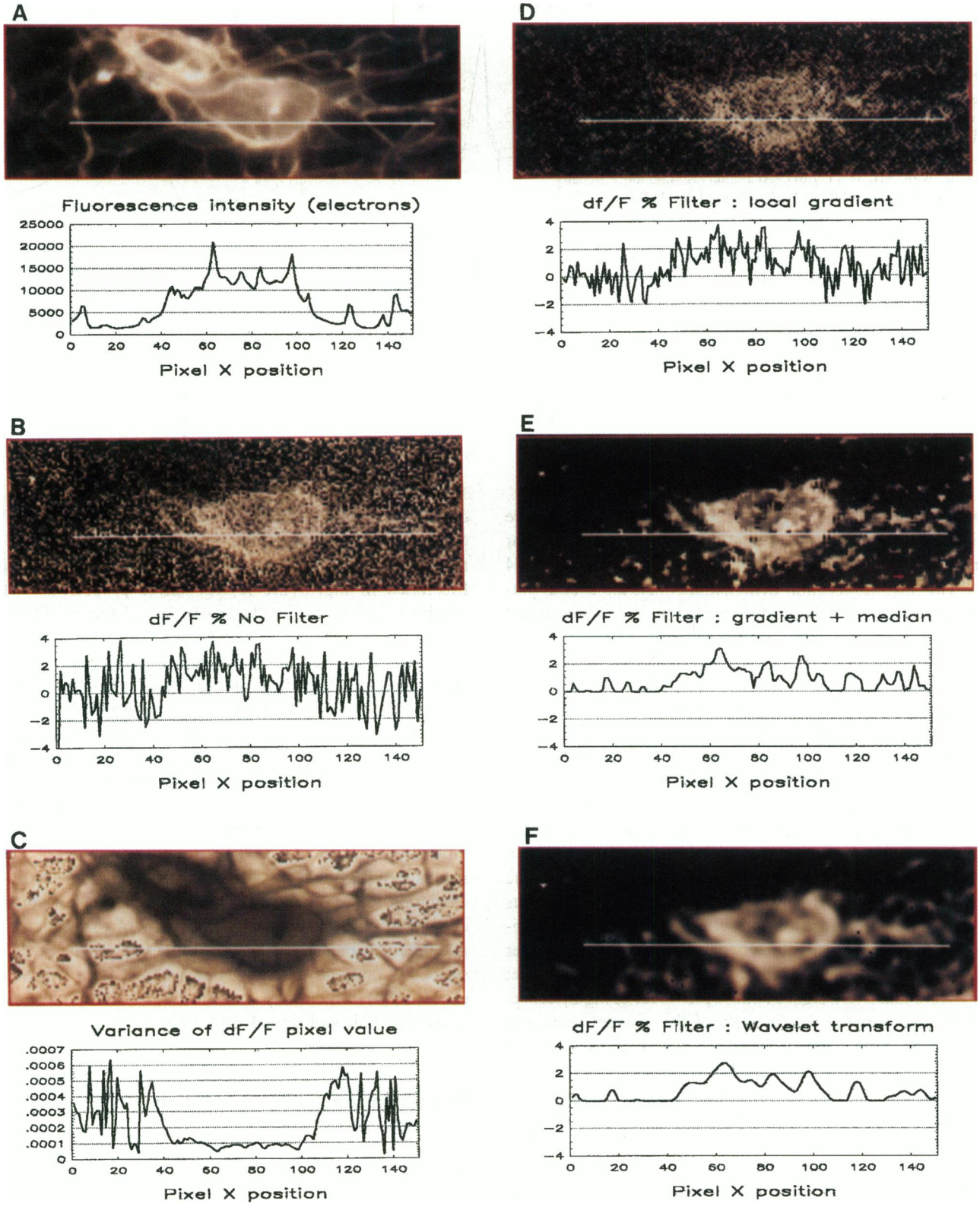


FIGURE 2 Image processing for detection of relative fluorescence changes produced by neuronal excitation. The curve below each image plots the intensity profile along the horizontal line (150 pixels) superimposed upon the image. (*A*) CCD fluorescence image of a nodose cell culture stained with the voltage-sensitive dye RH237 with an impaled neuron in the center, stimulated by 0.7-nA depolarizing current pulses (same neuron as in Fig. 4 *G* below). (*B*) Computed fractional fluorescence changes (d*F*/*F*%) image resulting from the excitation of the neuron in *A*. (*C*) Computed variance image. The intensity of every pixel is the variance of the corresponding pixel in the d*F*/*F* image *B*. (*D*) Image *B* after removal of background fluorescence noise removal by an outlier local gradient filter. (*E*) Image *B* after local gradient filter plus median filter (same neuron as in Fig. 4 *H*). (*F*) Image *B* after noise filtering and hierarchical structure detection by wavelet transform (same neuron as in Fig. 4 *K*).

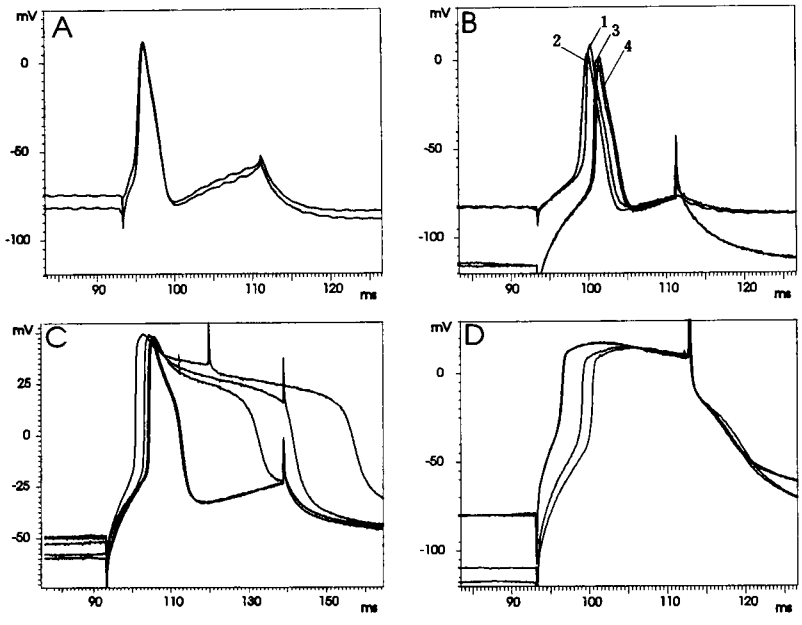


FIGURE 3 Intracellular recordings from cultured nodose neurons. Effects of staining and light exposure. (*A*) Action potentials (APs) evoked by depolarizing current pulses 5 min after penetration. (*B*) Action potentials recorded from the same neuron: AP1 after 10 min of staining with RH237 (1 $\mu$M); AP2 after 15 min of washing out the dye; AP3 and AP4 10 min later during two illuminations of 100 ms each. The neuron was held hyperpolarized at −115 mV. (*C*) Action potentials from another nodose neuron stained with RH237 (1 $\mu$M, 10 min) during five successive illuminations at 1-min intervals, showing the progressive broadening of the repolarization phase while the $Na^+$ fast component was unaffected. (*D*) Action potentials from another nodose neuron stained with RH237 (1.5 $\mu$M, 10 min) and recorded after multiple illuminations of the culture. Note the wide broadening of the repolarization phase.

tion. Finally, when an image was processed from a sequence for a neuron at rest, the resulting image displayed no cellular contours and was always devoid of significant signal (Fig. 4 *M*). This last observation demonstrates that the spatial patterns are directly related to the excitation of the neuron and excluded their production by uneven concentration of the dye or dye movements not correlated with the stimulation. The reliability of the clusters was further tested with a powerful mathematical tool, the wavelet transform. Briefly, the image was decomposed into several "wavelet planes," each plane containing objects of the original image observed at a different spatial resolution (Holdschneider et al., 1989, Starck and Bijaoui, 1994a,b). In each plane, truly uncorrelated noise was removed by rejection of all nonsignificant pixel intensities. The rejection, based on decision theory, operated by assuming that the intensity of all the pixels in each $dF/F$ image resulted only from noise, thus giving a Gaussian distribution with mean = 0 and a variance $\sigma^2$. Pixels with an intensity of an absolute value greater than $3.291\sigma$ had a probability of only 0.001% to be noise; they were taken as a signal with 99.9% level of significance. After noise removal the linearity of the wavelet transform allowed to reconstruct a filtered version of the original image that contained only statistically significant pixels. The resulting images are shown Fig. 4 *D*, *E* and *K*, *L*, which correspond to *B*, *C* and *H*, *J*, respectively. They display the same spatial distribution of the clusters as those revealed by the standard image processing used in *B*, *C*, *H*, and *J*. They demonstrate that the spatial patterns are highly significant statistically.

## Spatial pattern modification by blockade of the action potential

To determine whether the spatial patterns of depolarized sites were related to the activation of clusters of voltage-dependent channels operating during the time course of an action potential, experiments ($n$ = 20) were performed in the presence of tetrodotoxin (TTX) in the bathing solution. Illustrated in Fig. 5 are representative processed images obtained during the blockade of $Na^+$ channels. The two spatial patterns (Fig. 5 *D* and *E*) and corresponding action potentials (Fig. 5 *K*) recorded during the excitation of the single neuron (Fig. 5 *A* and *B*) were affected by local application of $10^{-6}$ M TTX, which suppressed the action potential within a few seconds (Fig. 5 *L*). The depolarized sites were reduced (Fig. 5 *F* and *G*). Recovery of the action potentials after TTX washout (Fig. 5 *M*) corresponded to a progressive reappearance of the depolarized sites in the images (Fig. 5 *H* and *J*) until a mosaic essentially comparable with that preceding TTX treatment emerged. These results indicated that the spatial patterns linked to neuronal excitation were somehow related to populations of voltage-dependent $Na^+$ channels. In this series of experiments no attempt was made to block other types of channels described in rat nodose neurons (Christian et al., 1994; Schild et al., 1994), which may explain the remaining clusters of depolarized sites observed with TTX.

## Spatial patterns with or without transmembrane current

It could be argued that the reduction of depolarized sites under TTX was due to the reduction in transmembrane potential produced by blockade of the action potential. To test further the voltage dependence of the clusters, experiments ($n$ = 16) were done under voltage-clamp conditions. Fig. 6 shows the image of an impaled neuron in a group of three (Fig. 6 *A* and *G*), producing an action potential (trace B in voltage recording *H*) with its corresponding spatial pattern of depolarized sites (Fig. 6 *B*). The surrounding

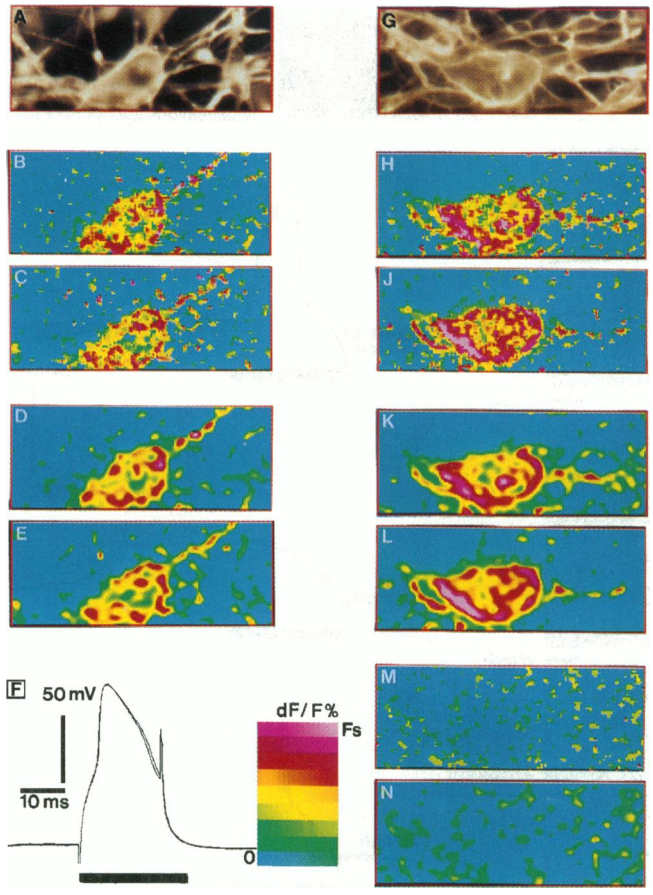


FIGURE 4 Spatial distribution of membrane depolarization sites during an action potential revealed by two different procedures of image processing. (*A*) CCD image of a nodose cell culture stained with RH 237 (0.5 μM; 10 min) using differential interference contrast (DIC) optics. An impaled neuron (resting potential: −80 mV at penetration) is seen in the center of the field surrounded by other cells and fine processes. (*B*), (*C*) d*F*/*F* changes in the same field as in *A*, during two successive action potentials (*F*) evoked at a time interval of 23 s. The image processing was performed with the local gradient method and median filtering. (*D*), (*E*) d*F*/*F* images obtained after noise rejection with wavelet transform, corresponding to images *B* and *C*, respectively. (*G*) Fluorescence image of another nodose culture with two adjacent stained neurons (RH 237; 0.5 μM; 10 min). The impaled neuron (resting potential: −52 mV at penetration) is in the center of the field (same neuron as in Fig. 2). (*H*), (*J*) d*F*/*F* changes in the same field as in *G* during two action potentials as in *F* (not shown) 14 s apart. Image processing was performed with the local gradient method and median filtering. (*K*), (*L*) d*F*/*F* images obtained after noise rejection with wavelet transform corresponding to images *H* and *J*, respectively. (*M*) d*F*/*F* image for the same field as in *G*, *H*, and *J*, with the neuron at rest. (*N*) d*F*/*F* image (neuron at rest) after noise rejection with wavelet transform. The black bar in *F* indicates the duration of the CCD shutter opening. The color scale reads from left to right and bottom to top. Each horizontal bar has a range value of 0.30% d*F*/*F* for *B* to *E* and 0.38% d*F*/*F* for *H* to *N*. Full scale is 2.68% for *B* to *E* and 3.3% for *H* to *N*. Depolarization is increasing toward red. Statistical significance between classes of colors: green (0.29–0.92%) to yellow (0.92–1.57%), yellow to red (1.57–2.60%) = 99.9% for *B* and *C*. For *H* and *J*, green (0.17–1.05%) to yellow (0.17–1.84%), yellow to red (1.84–3.30%) = 99.9%.

neurons displayed no significant signals, being faded in the field. When the impaled neuron was voltage clamped at a holding potential of −75 mV and stepped to −39 mV (trace C in voltage recording *J*), which was under threshold for activating an inward current (trace C in current recording *K*), the corresponding depolarized sites were greatly diminished (Fig. 6 *C*). Stepping the potential to −27 mV (trace D in voltage recording *J*) evoked an inward current (trace D in current recording *K*) with its corresponding spatial pattern (Fig. 6 *D*). The number of depolarized sites was greatly increased, revealing a pattern similar to that obtained during the action potential recorded under current-clamp conditions (Fig. 6 *B*). However, when a depolarizing voltage pulse (58 mV; trace E in voltage recording *J*) with the same magnitude and duration as the action potential (trace B in voltage recording *H*) was applied during local application of TTX ($10^{-6}$ M), the inward current was blocked (trace E in current recording *K*) and the corresponding number of depolarized sites was greatly decreased (Fig. 6 *E*). After the TTX was washed out from the bath solution, an incomplete recovery was recorded (trace F in current recording *K*), and the corresponding image (Fig. 6 *F*) showed an increased number of depolarized sites despite the identical amplitude (58 mV) of the depolarizing voltage pulse (trace F in voltage recording *J*). These results indicate that the dye response reflects local events resulting from the operations of ionic channels in the membrane rather than the overall transmembrane potential.

### Spatial patterns with channel inactivation

To examine further the relation of the spatial patterns to the working of ionic channels, we voltage clamped neurons to different holding potentials for 30–60 s and then stepped them for 20 ms with a constant 100-mV depolarizing pulse. An example of such an experiment is shown in Fig. 7. The holding potentials ranged from +7.8 to −106.9 mV, which should test for inactivation of voltage dependent sodium channels (plot *M*). The transmembrane current components (plot *L*) during the 100-mV step progressively increased as the holding potential became more negative. The corresponding processed d*F*/*F* images revealed an increase in the number of depolarized sites (plots *C* to *H*). The correlation between the number of depolarized sites with d*F*/*F* between 0.4% and 2.2% and the holding potential (plot *K*) strongly supports the interpretation that the depolarized sites revealed by the dye reflects channel activation.

## DISCUSSION

The optical system presented in this paper differs from other optical recording systems in that it gives no temporal information but provides topological maps of the excitation of single neurons. We simply give priority to the exploration of the spatial distribution of the local electrical events occurring in the membrane of excited neurons on the microscopic scale. One of the main reasons for using imaging microscopic technology as opposed to photodiode arrays to record optical signals is the potential for increased spatial resolu-

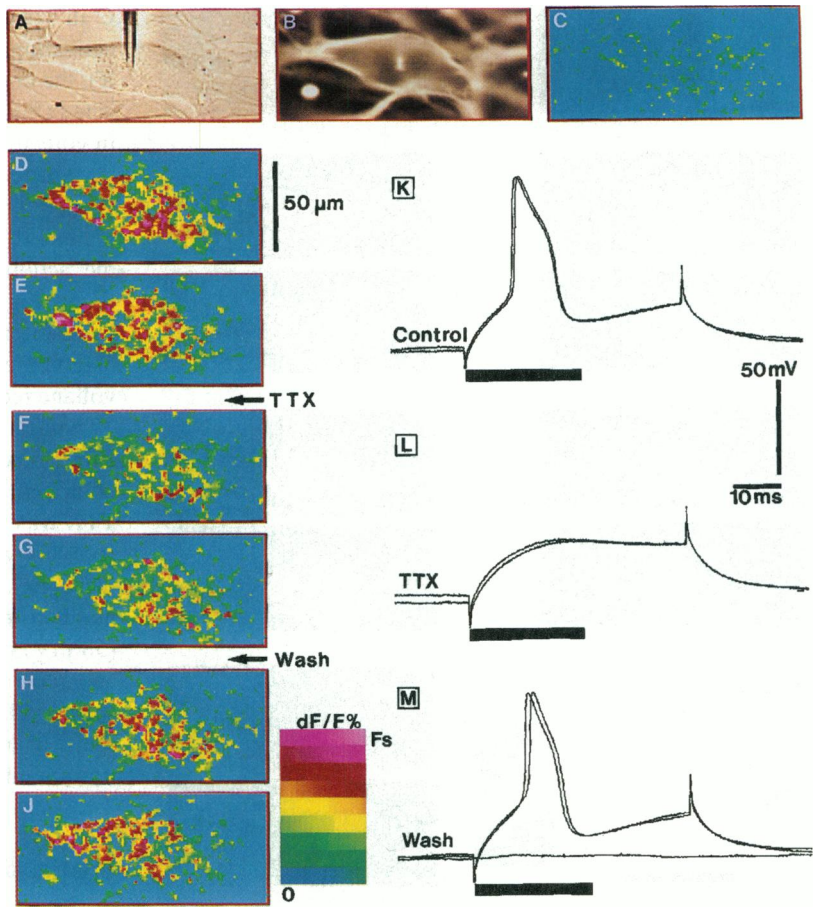


FIGURE 5 Effects of TTX on the spatial patterns of depolarized sites. (*A*) CCD image of an impaled nodose neuron (resting potential: −61 mV at penetration) using DIC optics. (*B*) Fluorescence image of the same field as in *A* after staining with RH 237 (1 μM; 10 min). (*C*) Processed d*F*/*F* image of the same field with the neuron at rest. (*D*), (*E*) Processed d*F*/*F* images of the excited neuron during intracellular stimulation (0.5 nA). The two images were obtained at a 20-s interval in synchrony with the two action potentials shown superimposed in *K* (resting potential −49 mV; overshoot +46 mV). Note very different patterns for virtually identical action potentials. (*F*), (*G*) Two successive processed d*F*/*F* images synchronized with intracellular recordings (*L*) after local application of $10^{-6}$ M TTX to block the rapid $Na^+$-dependent phase of the action potentials. (*H*), and (*J*) Processed d*F*/*F* images obtained at 32 and 55 s after the beginning of TTX washout from the bath. The spatial patterns reappeared progressively (compare *H* and *J*) with an increase in number of depolarized sites. (*M*) Immediate recovery of action potential generation (resting potential −44 mV; overshoot +45 mV). Black bars in *K* to *M* indicate the duration of the CCD shutter opening. The color scale reads from left to right and from bottom to top. Each horizontal bar has a range value of 0.28% d*F*/*F*. Full scale is 2.53%. Depolarization is increasing toward red. Statistical significance between classes of colors: green (0.20–0.90%) to yellow (0.90–1.46%), yellow to red (1.46–2.53%) = 99.9% for *D*, *E*, *H*, and *J* and 95% for *F* and *H*.

tion. Photodiode arrays record membrane areas of 100 $\mu m^2$, whereas with our system the pixel is 1 $\mu m^2$, allowing information to be obtained in a microscopic scale equivalent to the resolution of a patch-clamp microelectrode.

The main result emerging from this study is that the membrane of an excited neuron displays a patchy appearance in the microscopic scale of observation. This finding must be discussed in the context of the conventional notion that the potential difference between neighboring regions in the neuronal membrane must be small or negligible (isopotentiality) because of the long space constant (λ), in particular in the somatic region. The interpretation of this discrepancy requires that we evaluate critically possible sources of error.

First, the patchiness could result from noise in the measurements. The image processing used in this study is based on methods developed by astronomers to solve similar problems of instrumental and processing errors. In our conditions, all sources of noise are quantified. Then the statistical significance of the detected structures is evaluated, considering the total variance of each pixel in the image. Interestingly, the same patchy repartition of fluorescence sources is detected on the excited cell by two different methods: local gradient plus median filtering (Pratt, 1991), a nonlinear technique based on the measurement of the local properties of the image, and a linear procedure, the wavelet transform based on the analysis of hierarchized structures (Bijaoui, 1992; Starck and Bijaoui, 1994a,b). Both methods, which retain only signals with a high level of significance, lead to similar results, namely, the patchy repartition of fluorescence sources on the excited cell membrane, thus eliminating the problem of artifacts produced by noise in the measurements.

Second, the patchiness could result from dye redistribution in the membrane during the exposure time. This is easily checked by the computed images of the neuron at rest without intracellular stimulation in which a background without any cellular contours is displayed (see Figs. 4 *M* and *N*, 5 *C*, 6 *L*, and 7 *J*). Moreover, when an excited neuron is observed close to another cell that is not impaled, the latter cell disappears in the processed image during stimulation (see Figs. 4 and 6).

A last possibility would be a dye redistribution linked to the generation of the action potential in the observed impaled neuron. With a number of new techniques such as fluorescence photobleaching recovery it has become possible to measure the mobility of lipids and of many proteins in the plane of the cell membrane (for references, see Almers and Stirling, 1984). The time scale of the diffusion coefficients is in the range of seconds. This does not fit with the time course of an action potential and renders this explanation highly improbable.

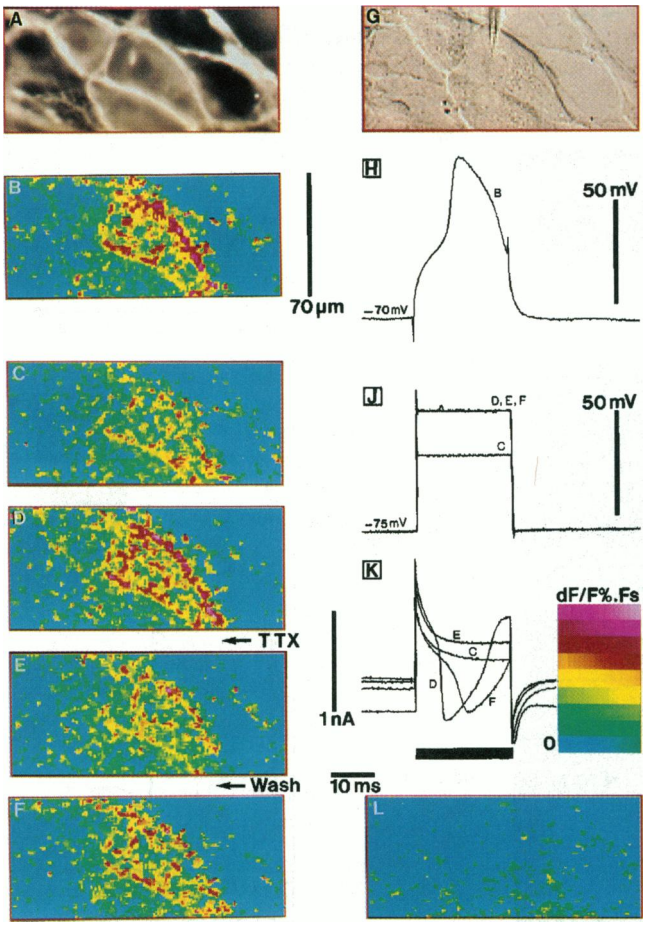


FIGURE 6 Depolarized sites spatial distribution under current and voltage-clamp conditions and during TTX blockade. (*A*) Fluorescence image of a nodose culture stained with RH237 (1.5 µM; 15 min) with three strongly labeled neurons. The impaled neuron (resting potential: −75 mV at penetration) is in the center of the field (DIC optics image *G*). (*B*) Processed d*F*/*F* image showing the spatial pattern of depolarized sites during an action potential (*H*). (*C*) The neuron is depolarized (trace C in voltage recording *J*) to just under threshold. No inward current is evoked (trace C in current recording *K*, leak and capacity current not subtracted). In (*D*) the applied voltage pulse is above threshold (trace D in voltage recording *J*) and evokes a fast inward current (trace D in current recording *K*). In (*E*) during the application of TTX ($10^{-6}$ M) in the bath, the fast inward current is blocked (trace E in current recording *K*). In (*F*) after TTX is washed out the fast inward current partially recovers (trace F in current recording *K*). (*L*) Processed d*F*/*F* image obtained when no stimulus is applied (neuron at rest). The black bar at the bottom of electrical recordings indicates the duration of the CCD shutter opening. The color scale reads from left to right and from bottom to top. Each horizontal bar has a range value of 0.25% d*F*/*F*. Full scale is 2.25%. Depolarization is increasing toward red. Statistical significance between classes of colors: green (0.19–0.78%) to yellow (0.78–1.30%), yellow to red (1.30–2.25%) = 99.9% for *B*, *D*, *E*, and *F* and 95% for *C*.

The explanation of the membrane patchiness is easily found when the conventional electrophysiological recordings are compared with our optical recordings. Intracellular microelectrodes, photodiodes, or both record the space integral of electrical events with very high temporal resolution but provide no information on the spatial distribution of these events; microelectrodes register membrane as isopotential. In contrast, our optical observations have virtually no temporal resolution but provide information on the spatial distribution of local membrane potential over large areas of somatic and neuritic membrane. They provide the time integral of the electrical events observed at a resolution in the micrometer range. Under these conditions the membrane is very evidently not isopotential. At that level of high spatial resolution we deal essentially with local transient events linked to the stochastic operations of populations of channels. An action potential produces a patchy distribution of local potential changes, and a second action potential in the same cell that is electrophysiologically indistinguishable from the first nevertheless produces a different spatial distribution of local depolarizations. Because of the negligible temporal resolution in our approach, we can say nothing about how local membrane potential fluctuates over the course of an action potential. For example, we cannot determine whether local potential changes begin close to the site of current injection and then spread from there into the neurites or whether scattered sites of depolarization occur simultaneously over the neuron membrane. Ideally, to tackle questions such as this would require a technology capable of providing simultaneous patch-clamp recordings from multiple sites on the surface of an individual neuron.

One proposal that can accommodate our observations is that the dye acts as an electric field sensor. Fluorescence voltage-sensitive dyes were introduced by Loew et al. (1979) as electrochromic dyes for optical recording of membrane potentials. It is well established that styril and other such dyes respond to the overall membrane potential perhaps exclusively. This conclusion is based mainly on the results published in the early Cohen group papers (Cohen et al., 1974; Ross et al., 1977). They showed that optical signals recorded with photodiodes depended in some manner on changes in the transmembrane potential when obtained with millisecond potential steps around the resting potential, in voltage-clamped squid giant axons. But there are reports that these probes may respond to local field changes that are not related to changes in global transmembrane voltages (Aiuchi and Kobatake, 1979; Beeler et al., 1981; Krasne, 1983; Bedlack et al., 1994). Recently Heiny and Jong (1990) reported that the dye WW375, which belongs to the merocyanine-rhodamine class of voltage-sensitive dyes, responds with an unexpected nonlinearity to voltage changes across the T-tubular membrane. They proposed that the dye responds to local electrostatic potential changes. These potentials would neither be controlled by voltage clamp nor extend beyond molecular distances from the membrane. The possibility that the voltage response of styril dye contains nonelectrochromic components has also been discussed by Fluhler et al. (1985) and Müller et al. (1986). Further evidence is found in voltage-sensitive dye studies of charge translocation in the plasma membrane (Apell et al., 1987; Stürmer et al., 1989). Klodos and Forbush (1988) reported that the styril dye RH160 incorporated into Na, K-ATPase containing membrane monitors transitions between states of the pumping cycles. More recently

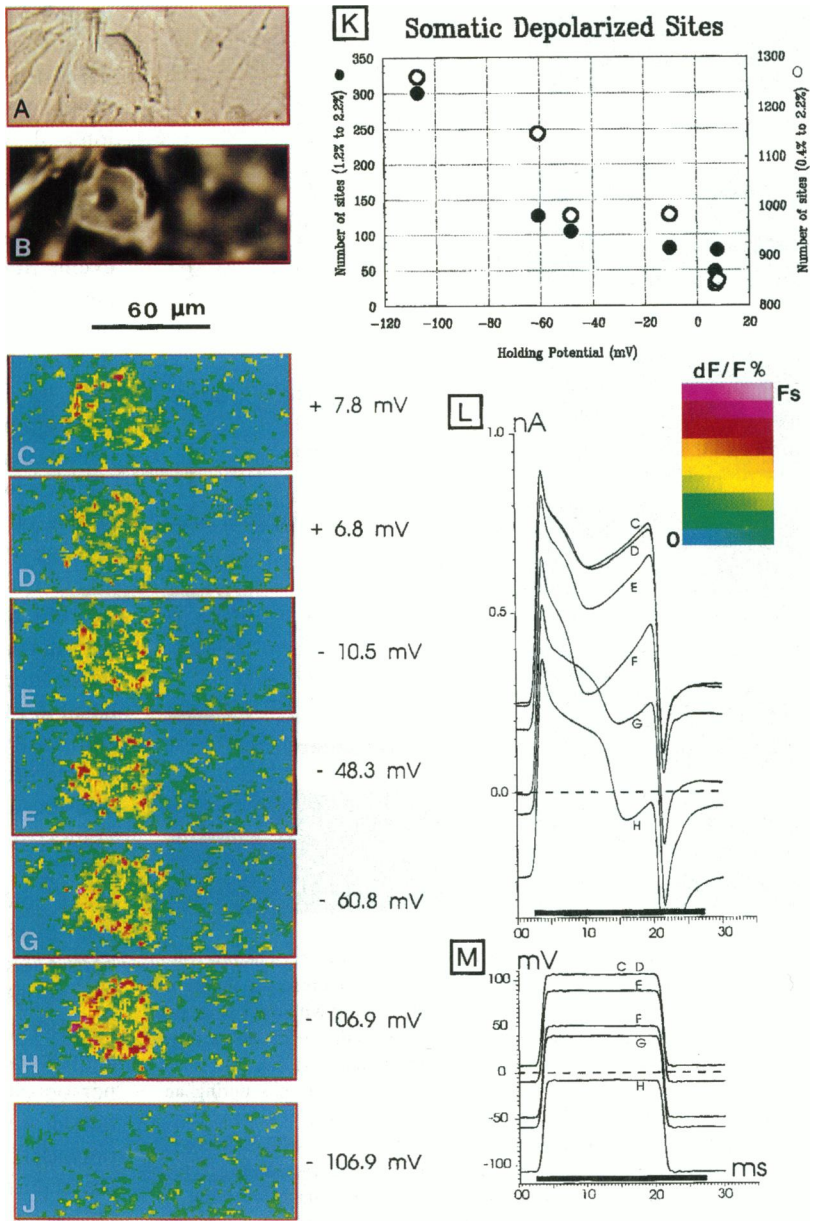


FIGURE 7 Spatial patterns with inactivation of voltage-dependent channels. (*A*) CCD image of an impaled neuron (resting potential: −46 mV at penetration) with DIC optics. (*B*) Fluorescence image of the same field with the stained neuron (RH237; 1 µM; 10 min). (*C*) to (*H*) Processed d*F*/*F* images of the same field taken at different holding potentials as indicated, with constant step depolarization (100 mV) of the impaled neuron. (*J*) Processed d*F*/*F* image of the same neuron at a holding potential of −106.9 mV without step depolarization. (*K*) Plots of the number of depolarized sites in images *C* to *H* against the corresponding holding potential. Filled circles are the number of depolarized sites over the neuron in the range of 1.4% to 2.3% (*left ordinates scale*); open circles are the total number of depolarized sites in the range of 0.4% to 2.3% (*right ordinates scale*). (*L*) Current recordings corresponding to images *C* to *H* (leak and capacity current not subtracted). (*M*) Depolarizing voltage steps (100 mV) applied at different holding potentials during recording of images *C* to *H*. The Black bars in *L* and *M* indicate the duration of the CCD shutter opening. The color scale reads from left to right and bottom to top. Each horizontal bar has a range value of 0.25%. Full scale is 2.25%. Depolarization is increasing toward red. Statistical significance between classes of colors: green (0.19–0.78%) to yellow (0.78–1.30%) = 99.9% for *C*–*H*, yellow to red (1.30–2.25%) = 95% for C–G, and 99.9% for H.

Bühler et al. (1991) presented evidence that two styril dyes, RH421 and RH237 (used in this series of experiments), respond to changes of the electric field strength in the membrane resulting from charge movements during the pumping cycle. They have investigated the possible origin of the fluorescence changes and concluded that the most likely explanation is that the dye acts as a field sensor.

If this proposal is correct, the present findings can be interpreted as the result of imaging the dye response to local changes of electric field strength resulting from charge movements in the membrane-spanning proteins. In particular, our experiments under voltage-clamp conditions with TTX blockade or channel inactivation favor this interpretation. The presence of transmembrane current is accompanied by patchiness in the membrane. Conversely, after blockade of current by TTX or channel inactivation, the reduction in the number of depolarized sites shows that, under our recording conditions, it is the operation of the channels that evokes the dye response, inasmuch as the applied depolarizing voltage step has a negligible effect in itself.

Although the mechanism of the dye response remains unknown and is not a problem that can be dealt with in the present study, two different origins have been proposed. The dye may bind directly to the integral membrane proteins and become sensitive to conformational changes in these proteins (see Klodos and Forbush, 1988; Stürmer et al., 1989) or the dye molecules incorporated into the lipid bilayer regions of the membrane may sense changes in local electric fields (see Bühler et al., 1991).

If the latter hypothesis is correct, then the patchiness of the membrane observed during the generation of an action potential may result from the nonhomogeneous spatial distribution

of voltage-dependent channels. Such heterogeneity was shown in the left giant cell of *Aplysia* by the use of local current recordings from different regions of the membrane (Kado, 1973). It is now widely accepted that the membrane is a mosaic of bilayer domains and embedded proteins and that the dielectric properties of the membrane are nonhomogeneous. Recent data suggest the tendency of channels to cluster, the relative differences of channel density or occurrence of different conductances between two regional membrane areas, and that channel clustering plays a physiological role (see, for example, Huguenard et al., 1989; Robitaille et al., 1990; Regehr and Tank, 1990; Silver et al., 1990; Arancio and MacDermott, 1991; Müller and Connor, 1991; Llinás et al., 1992; Usowicz et al.; Shapiro, 1993; and, for references, Fraser and Poo, 1982; Almers and Stirling, 1984). These observations fit with our processed images displaying a nonuniform spatial distribution of depolarized sites in the microscopic scale.

The variability of this patterned membrane topography observed from trial to trial is not in contradiction with the fact that single-site recorded macroscopic electrical events remain similar. Recent studies (DeFelice and Isaac, 1992; Fox and Lu, 1994) have revealed that global coupling across large spatial membrane areas enables clusters of stochastic ion channels to produce stable macroscopic electrical events such as resting potentials and action potentials. During excitation, a given number of channels must open, but, in view of the stochastic behavior of channels, there is no reason to expect the same channels located in the same membrane region to open from trial to trial. If this last remark is true, the variability of the spatial pattern would favor our interpretation of small clusters of active channels as the origin of the depolarized sites.

We thank Drs. L. B. Cohen, P. Meyrand, and A. J. Simmers for critical reading of previous versions of the manuscript. We are particularly indebted to Drs. H. R. Lüscher and M. Rioult for friendly advice, technical help, and provocative discussions during the years of implementation of our optical system. We are very grateful to Drs. A. Bijaoui, Astronome du Roy for guiding the adaptation of astronomical image processing, P. Combe for discussion of statistical analysis, and A. R. Lieberman for encouragement and for critically reviewing an early version of our manuscript. We are also grateful to Dr. R. T. Kado for many stimulating discussions and for scrutinizing the revised version of this paper. This work was supported by CNRS and INSERM grants and also by MRE (grants 90.C.00978 and 91.C.0946), C.E.E. (grant SCI-225C). Yasmina Chitti is supported by the MRE. Ingrid Schmiedel-Jakob was a fellow of INSERM (1989), CNRS (1991), and FRM (1992).

## REFERENCES

Aiuchi, T., and Y. Kobatake. 1979. Electrostatic interaction between merocyanine 540 and liposomal and mitochondrial membranes. *J. Membr. Biol.* 45:233–244.

Almers, W., and C. Stirling. 1984. Distribution of transport proteins over animal cell membranes. *J. Membr. Biol.* 77:169–186.

Apell, H. J., R. Borlinghaus, and P. Laüger. 1987. Fast charge translocation associated with partial reactions on the Na, K-pump: II. Microscopic analysis of transient currents. *J. Membr. Biol.* 97:179–191.

Arancio, O., and A. B. MacDermott. 1991. Differential distribution of excitatory amino acid receptors on embryonic rat spinal cord neurons in culture. *J. Neurophysiol.* 65:899–913.

Baccaglini, P., and E. Cooper. 1982. Electrophysiological studies of new-born rat nodose neurones in cell culture. *J. Physiol. (London).* 324:429–439.

Bacskai, B. J., B. Hochner, M. Mahaut-Smith, S. R. Adams, B. K. Kaang, E. R. Kandel, and R. Y. Tsien. 1993. Spatially resolved dynamics of cAMP and protein kinase A subunits in *Aplysia* sensory neurons. *Science.* 260:222–226.

Bedlack, R. S. Jr., Mei-de Wei, S. H. Fox, E. Gross, and L. M. Loew. 1994. Distinct electric potentials in soma and neurite membranes. *Neuron.* 13:1187–1193.

Beeler, T. J., R. H. Farmen, and A. N. Martonosi. 1981. The mechanism of voltage-sensitive dye responses on sarcoplasmic reticulum. *J. Membr. Biol.* 62:113–137.

Bijaoui, A. 1992. Analysis of hierarchized structures in astronomy. *Nuclear Phys.* A545:409c–418c.

Bühler, R., W. Stürmer, H. J. Apell, and P. Läuger. 1991. Charge translocation by the Na, K-pump: I. Kinetics of local field changes studied by time-resolved fluorescence measurements. *J. Membr. Biol.* 121:141–161.

Catterall, W. A. 1988. Structure and function of voltage-sensitive ion channels. *Science.* 242:50–61.

Chien, C. B., and J. Pine. 1991. Voltage-sensitive dye recording of action potentials and synaptic potentials from sympathetic microcultures. *Biophys. J.* 60:697–711.

Chitti, Y., S. Tyč-Dumont, P. Gogan, and A. Bijaoui. 1995. Neurobiologie: détection à haute résolution spatiale de faibles signaux sur des images à variance hétérogène. *In* Imagerie Scientifique et Traitement d'Image. First International Symposium, AAAF, Cannes, France, 4–6 April 1995. m1–m17.

Christian, E. P., J. Togo, and K. E. Naper. 1994. Guinea-pig visceral C-fiber neurons are diverse with respect to the $K^+$ currents involved in action-potential repolarization. *J. Neurophysiol.* 71:561–574.

Cohen, L. B., B. M. Salzberg, H. V. Davila, W. N. Ross, D. Landowne, A. S. Waggoner, and C. H. Wang. 1974. Changes in axon fluorescence during activity: molecular probes of membrane potential. *J. Membr. Biol.* 19:1–36.

Cohen, L., H. P. Höpp, J. Y. Wu, C. Xiao, J. London, and D. Zecevic. 1989. Optical measurement of action potential activity in invertebrate ganglia. *Ann. Rev. Physiol.* 51:527–541.

Connor, J. A. 1986. Digital imaging of free calcium changes and of spatial gradients in growing processes in single, mammalian central nervous system cells. *Proc. Natl. Acad. Sci. USA.* 83:6179–6183.

DeFelice, L. J., and A. Isaac. 1992. Chaotic states in a random world: relationship between the nonlinear differential equations of excitability and the stochastic properties of ion channels. *J. Stat. Phys.* 70:339–354.

Fluhler, E., V. G. Burnham, and L. M. Loew. 1985. Spectra, membrane binding, and potentiometric responses of new charge shift probes. *Biochemistry.* 24:5749–5755.

Fox, R. F., and Y. N. Lu. 1994. Emergent collective behavior in large numbers of globally coupled independently stochastic ion channels. *Phys. Rev.* 49:3421–3431.

Fraser, S. E., and Mu-ming Poo. 1982. Development, maintenance and modulation of patterned membrane topography: models based on the acetycholine receptor. *Curr. Top. Dev. Biol.* 17:77–100.

Fromherz, P., H. H. Dambacher, H. Ephardt, A. Lambacher, C. O. Müller, R. Neigl, H. Schaden, O. Schenk, and T. Vetter. 1991. Fluorescent dyes as probes of voltage transients in neuron membranes. Progress Report. *Ber. Bunsenges. Phys. Chem.* 95:1333–1344.

Gallego, R., and C. Eyzaguirre. 1978. Membrane and action potential characteristics of A and C nodose ganglion cells studied in whole ganglia and in tissue slices. *J. Neurophysiol.* 41:1217–1232.

Gogan, P., J. P. Ternaux, and S. Tyč-Dumont. 1991. Hétérogénéité de l'activation membranaire des neurones et de la glie de mammifère montrée in vitro par une visualisation quantitative. *C.R. Acad. Sci. Paris, Ser. D.* 312:547–554.

Gogan, P., and S. Tyč-Dumont. 1994. High spatial resolution imaging of electrical activity of single neurons in culture. Proc. III FAOPS Congress, Shanghai, 7–10 November. p. 249, S13–19 (P).

Grinvald, A., R. Hildesheim, I. C. Farber, and L. Anglister. 1982. Improved fluorescent probes for the measurement of rapid changes in membrane potential. *Biophys. J.* 39:301–308.

Grinvald, A., A. Fine, I. C. Farber, and R. Hildesheim. 1983. Fluorescence monitoring of electrical responses from small neurons and their processes. *Biophys. J.* 42:195–198.

Grinvald, A., R. D. Frostig, E. Lieke, and R. Hildesheim. 1988. Optical imaging of neuronal activity. *Physiol. Rev.* 68:1285–1366.

Gross, D., L. M. Loew, and W. W. Webb. 1986. Optical imaging of cell membrane potential changes induced by applied electric fields. *Biophys. J.* 50:339–348.

Grossmann, A., and J. Morlet. 1985. Mathematics and Physics, Lecture on Recent Results. World Scientific, Singapore.

Heiny, J. A., and D. Jong. 1990. A nonlinear electrostatic potential change in the T-system of skeletal muscle detected under passive recording conditions using potentiometric dyes. *J. Gen. Physiol.* 95:147–175.

Higashi, H., K. Morita, and R. North. 1984. Calcium-dependent after potentials in visceral afferent neurons of the rabbit. *J. Physiol. (London).* 355:479–492.

Hille, B. 1992. Ionic Channels of Excitable Membranes, 2nd ed. Sinauer Associates, Inc., Sunderland, MA.

Holdschneider, M., R. Kronland-Martinet, J. Morlet, and P. Tchamitchian. 1989. A real-time algorithm for signal analysis with the help of the wavelet transform *In* Wavelets. J. M. Combes et al., editors. Springer-Verlag, Berlin. 286–297.

Huguenard, J. R., O. P. Hamill, and D. A. Prince. 1989. Sodium channels in dendrites of rat cortical pyramidal neurons. *Proc. Natl. Acad. Sci. USA.* 86:2473–2477.

Ikeda, S. R., G. G. Schofield, and F. F. Weight. 1986. $Na^+$ and $Ca^{2+}$ currents of acutely isolated adult rat nodose ganglion cells. *J. Neurophysiol.* 55:527–539.

Kado, R. T. 1973. Aplysia giant cell: soma-axon voltage clamp current differences. *Science.* 182:843–845.

Klodos, I., and B. Forbush. 1988. Rapid conformational changes of the Na/K pump revealed by a fluorescent dye, RH-160. *J. Gen. Physiol.* 92:46a (abstract).

Krasne, S. 1983. Interactions of voltage-sensing dyes with membranes: III. Electrical properties induced by merocyanine 540. *Biophys. J.* 44: 305–314.

Llinás, R. 1988. The intrinsic electrophysiological properties of mammalian neurons: insights into central nervous system function. *Science.* 242:1654–1664.

Llinás, R., M. Sugimori, and R. B. Silver. 1992. Microdomains of high calcium concentration in a presynaptic terminal. *Science.* 256:677–679.

Loew, L. M., S. Scully, L. Simpson, and A. S. Waggoner. 1979. Evidence for a charge shift electrochromic mechanism in a probe of membrane potential. *Nature (London).* 281:497–499.

Midtgaard, J., N. Lasser-Ross, and W. N. Ross. 1993. Spatial distribution of $Ca^{2+}$ influx in turtle purkinje cell dendrites in vitro: role of a transient outward current. *J. Neurophysiol.* 70:2455–2469.

Miller, C. 1991. 1990: annus mirabilis of potassium channels. *Science.* 252:1092–1096.

Miyakawa, H., V. Lev-Ram, N. Lasser-Ross, and W. N. Ross. 1992. Calcium transients evoked by climbing fiber and parallel fiber synaptic inputs in guinea-pig cerebellar Purkinje neurons. *J. Neurophysiol.* 68: 1178–1189.

Müller, W., and J. A. Connor. 1991. Cholinergic input uncouples $Ca^{2+}$ changes from $K^+$ conductance activation and amplifies intradendritic $Ca^{2+}$ changes in hippocampal neurons. *Neuron.* 6:901–905.

Müller, W., H. Windisch, and H. A. Tritthart. 1986. Fluorescent styryl dyes applied as fast optical probes of cardiac action potential. *Eur. Biophys. J.* 14:103–111.

Parzen, 1960. Modern Probability Theory and Its Applications. John Wiley & Sons, New York.

Pratt, W. K. 1991. Digital Image Processing, 2nd ed. John Wiley & Sons, New York.

Regehr, W. G., J. A. Connor, and D. W. Tank. 1989. Optical imaging of calcium accumulation in hippocampal pyramidal cells during synaptic activation. *Nature (London).* 341:533–536.

Regehr, W. G., and D. W. Tank. 1990. Postsynaptic NMDA receptor-mediated calcium accumulation in hippocampal CA1 pyramidal cell dendrites. *Nature (London).* 345:807–810.

Rioult, M. G., P. Gogan, H. R. Lüscher, and S. Tyč-Dumont. 1991. Spatial and temporal optical recording of the excitation of single neurons combining a cooled CCD and a photodiode array. 21st Annual Meeting of the Society for Neuroscience, New Orleans, 10–15 November 1991. *Abstracts Soc. Neurosci.* 17:n 408.3.

Robitaille, R., E. M. Adler, and M. P. Charlton. 1990. Strategic location of calcium channels at transmitter release sites of frog neuromuscular synapses. *Neuron.* 5:773–779.

Ross, W. N., B. M. Salzberg, L. B. Cohen, A. Grinvald, H. V. Davila, A. S. Waggoner, and C. H. Chang. 1977. Changes in absorption, fluorescence, dichroism and birefringence in stained axons: optical measurement of membrane potential. *J. Membr. Biol.* 33:141–183.

Ross, W. N., N. Lasser-Ross, and R. Werman. 1990. Spatial and temporal analysis of calcium-dependent electrical activity in guinea-pig Purkinje cell dendrites. *Proc. R. Soc. London Ser. B.* 240:173–185.

Schild, J. H., J. W. Clark, M. Hay, D. Mendelowitz, M. C. Andersen, and D. L. Kunze. 1994. A- and C-type rat nodose sensory neurons: model interpretations of dynamic discharge characteristics. *J. Neurophysiol.* 71:2338–2358.

Schilling, K., M. H. Dickinson, J. A. Connor, and J. I. Morgan. 1991. Electrical activity in cerebellar cultures determines purkinje cell dendritic growth patterns. *Neuron.* 7:891–902.

Schmiedel-Jakob, I., J. P. Ternaux, and P. Portalier. 1992. Electrical membrane characteristics of neonatal rat nodose ganglion cells in primary culture. *Eur. J. Neurosci.* suppl. 5:Abstract 4198.

Shapiro, L. 1993. Protein localization and asymmetry in the bacterial cell. *Cell.* 73:841–855.

Silver, R. A., A. G. Lamb, and S. R. Bolsover. 1990. Calcium hotspots caused by L-channel clustering promote morphological changes in neuronal growth cones. *Nature (London).* 343:751–754.

Slezak, E., V. de Lapparent-Gurriet, and A. Bijaoui. 1993. Objective detection of voids and high density structures in the first CfA redshift survey slice. *Astrophysical J.* 409:517–529.

Starck, J. L., and A. Bijaoui. 1994a. Filtering and deconvolution by the wavelet transform. *Signal Processing.* 35:195–211.

Starck, J. L., and A. Bijaoui. 1994b. Multiresolution deconvolution. *J. Opt. Soc. Am. A.* 11:1580–1588.

Stühmer, W. 1991. Structure-function studies of voltage-gated ion channels. *Ann. Rev. Biophys. Biophys. Chem.* 20:65–78.

Stürmer, W., H. J. Apell, I. Wuddel, and P. Läuger. 1989. Conformational transitions and charge translocation by the Na, K-pump: comparison of optical and electrical transients elicited by ATP-concentration jumps. *J. Membr. Biol.* 110:67–86.

Sugimori, M., and R. Llinás. 1990. Real-time imaging of calcium influx in mammalian cerebellar purkinje cells in vitro. *Proc. Natl. Acad. Sci. USA.* 87:5084–5088.

Tauc, L., editor. 1992. Calcium and intraneuronal signalling. 16th Gif Lecture in Neurobiology. *J. Physiol. Paris.* 86:1–155.

Tukey, J. W. 1971. Exploratory Data Analysis. Addison-Wesley, Reading, MA.

Unwin, N. 1989. The structure of ion channels in membranes of excitable cells. *Neuron.* 3:665–676.

Usowicz, M. M., M. Sugimori, B. Cherksey, and R. Llinás. 1992. P-type calcium channels in the somata and dendrites of adult cerebellar purkinje cells. *Neuron.* 9:1185–1199.

Verderio, C., S. Coco, G. Fumagalli, and M. Matteoli. 1994. Spatial changes in calcium signalling during the establishment of neuronal polarity and synaptogenesis. *J. Cell Biol.* 126:1527–1536.

Wadman, W. J., and J. A. Connor. 1992. Persisting modification of dendritic calcium influx by excitatory amino acid stimulation in isolated CA1 neurons. *Neuroscience.* 48:293–305.

Worrall, D. M., C. Biemesderfer, and J. Barnes, editors. 1992. Astronomical Data Analysis Software and Systems I. Astronomical Society of the Pacific Conference series, Vol. 25. Book Crafters, Inc., San Francisco, CA.

Zheng, J. Q., M. Felder, J. A. Connor, and Mu-ming Poo. 1994. Turning of nerve growth cones induced by neurotransmitters. *Nature (London).* 368:140–142.